



## Synthesis of platinum nanoclusters and electrochemical investigation of their stability



R.A. Hackendorn, Anil V. Virkar\*

Department of Materials Science & Engineering, 122 S. Central Campus Drive, University of Utah, Salt Lake City, UT 84112, USA

### HIGHLIGHTS

- Investigated electrochemical coarsening in Pt nanoclusters.
- Studied the effect of the initial particle size distribution on growth kinetics.
- Narrow particle size distribution minimizes thermodynamic driving force for growth.
- Narrower the initial catalyst size distribution, the greater is their stability.

### ARTICLE INFO

#### Article history:

Received 12 February 2013

Received in revised form

6 May 2013

Accepted 8 May 2013

Available online 16 May 2013

#### Keywords:

PEM fuel cells

Catalyst growth

Size distribution

Mono-dispersed catalysts

### ABSTRACT

Platinum nanoclusters were synthesized using two methods: (a) ascorbic acid reduction of  $K_2PtCl_6$ , (b) an  $H_2PtCl_6$  polyol process. Both processes yield clusters of platinum consisting of nanoparticles with a narrow size distribution. Experiments were conducted using platinum nanoclusters as the working electrode and bulk platinum wire as the counter electrode, both supported on inert, electronically conducting substrates. The electrodes were immersed in a  $PtCl_4$  + dimethyl sulfoxide electrolyte solution. The spacing between the electrodes was maintained at 1 mm or 6 mm. Electrical potential was measured across the two electrodes as a function of time. The samples (scraped off the nano-electrode) were examined using transmission electron microscopy (TEM). Experimental data show significantly lower kinetics of particle growth for the nanoclustered, uniformly sized particles as compared to commercially available carbon-supported platinum catalysts.

© 2013 Elsevier B.V. All rights reserved.

## 1. Introduction

The use of nanoparticles for catalytic applications has grown significantly over the last few decades, with particular emphasis on platinum. In many applications, however, the particles grow in size leading to a loss of catalytic activity. In several cases, the degradation kinetics are not fully understood. The principal objective of this work was to investigate the mechanism or mechanisms of the growth of nanoclustered platinum particles immersed in a liquid containing a dissolved Pt salt. Investigation of the growth of nanoparticles in a nanocluster also should allow elucidation of the role of coupled transport and the role of adjacent liquid on transport kinetics. One of the applications of Pt and Pt–alloy nanoparticles as a catalyst is in proton exchange membrane fuel cells (PEMFC). Some of the known modes of catalyst degradation in PEMFC are: (a) catalyst particle detachment from the support, (b)

agglomeration/sintering, (c) Ostwald ripening, and (d) transport and precipitation into the membrane [1–12]. While many researchers have investigated these degradation mechanisms, few have addressed the effect of the initial particle size distribution on the kinetics of particle growth. An exception to this is a recent study by Popescu et al. who investigated the effect of initial particle size distribution of size-selected gold atomic clusters supported on carbon on the kinetics of growth when aged in air [13]. To the authors' knowledge, no such studies in any medium on platinum nanoparticles have been reported.

Many commercially available Pt or Pt alloy catalysts are ~1–6 nm in diameter and dispersed on a high surface area carbon support. In Ostwald ripening and agglomeration/sintering (Fig. 1), the driving force for growth is directly related to the reduction in surface energy accompanying particle growth. While many catalysts are metallic, such as platinum, in several electrochemical devices the medium in which the catalyst particles are submerged is almost always a nonmetallic liquid. Thus, the transport of Pt during growth involves the transport of ions (e.g.  $Pt^{2+}$  and/or  $Pt^{4+}$ ) through the medium and a parallel (coupled) transport of electrons through the support which

\* Corresponding author. Tel.: +1 801 581 5396; fax: +1 801 581 4816.

E-mail address: [anil.virkar@utah.edu](mailto:anil.virkar@utah.edu) (A.V. Virkar).

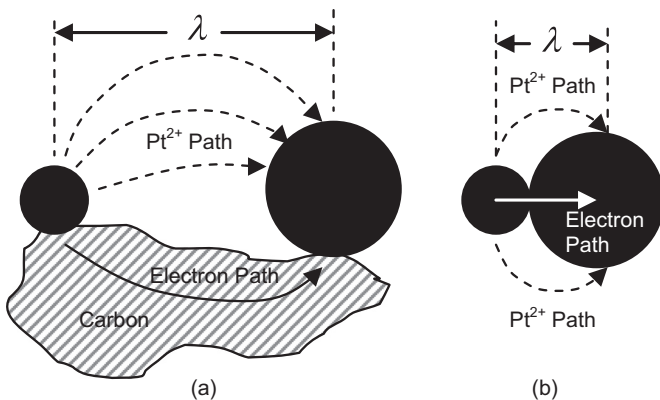


**Fig. 1.** Mechanism of particle growth in PEMFC by: (a) Ostwald ripening, (b) agglomeration/sintering. Both occur by a coupled transport of Pt<sup>2+</sup> (and/or Pt<sup>4+</sup>) ions through ionomer/aqueous media and electron transport through the electron conductor (or through direct contact). Net Pt transport occurs from smaller particles to larger particles.

is usually an electronic conductor such as carbon [14]. The net transport of Pt thus necessitates a coupled transport of Pt ions (Pt<sup>2+</sup> and/or Pt<sup>4+</sup>) through ionomer/aqueous medium and of electrons through the carbon support [14]. For particles that are immersed in a liquid medium and are also in physical contact, coupled transport involves the transport of Pt<sup>2+</sup>/Pt<sup>4+</sup> through the liquid and electron transfer through direct particle to particle contact. It is important to note that in most cases in which the temperature is low (e.g. room temperature), even for metallic nanoparticles in direct contact negligible transport occurs by a solid state mechanism (such as surface diffusion or bulk diffusion) due to the very low surface or bulk diffusion coefficients compared to ionic diffusion coefficients in liquids. For example, at room temperature the diffusion coefficient of Pt<sup>2+</sup>/Pt<sup>4+</sup> in liquid media is  $\sim 10^{-6} \text{ cm}^2 \text{ s}^{-1}$ , while the solid state surface diffusion coefficient of Pt measured at room temperature is only on the order of  $10^{-19} \text{ cm}^2 \text{ s}^{-1}$ , or some 13 orders of magnitude lower [15].

In this work, platinum nanoclusters were synthesized to study the kinetics of particle growth in an ion-conducting medium involving a coupled transport. The driving force for growth is related to differences in the chemical potentials of adjacent particles and can be given by the Gibbs–Thomson equation, according to which the smaller the particle size the higher is the chemical potential [16]. Typically, the size variation among the individual Pt particles provides a sufficient chemical potential difference and is the driving force for Ostwald ripening/particle coarsening. In the case of nanoclustered platinum catalyst particles, the size variation in the nanoparticles residing on the surface of the nanoclusters is expected to provide the driving force for their growth. If the particle size distribution is narrow, the driving force will be small, and this should lead to a lowering of the kinetics of particle growth.

Two processes were used for the synthesis of nanoclustered platinum particles; an ascorbic acid reduction process and a polyol process [17,18]. Both processes are fairly simple to use and lead to platinum nanoclusters composed of nanoparticles roughly 3–5 nm in diameter. However, the polyol process produces a very noticeable layer of platinum on the substrate (many nanoclusters form chains), while the ascorbic acid reduction process tends to yield individual nanoclusters that are evenly distributed. Two different types of substrates were used upon which platinum nanoclusters were deposited. These substrates with platinum nanoclusters served as the working electrode. A platinum wire wrapped around another identical substrate served as the counter electrode. The experimental procedure, results, and discussion are presented in what follows.

## 2. Experimental procedure

### 2.1. Materials

K<sub>2</sub>PtCl<sub>4</sub> (99.9%), PtCl<sub>4</sub> (99.99%), and dimethyl sulfoxide (DMSO) (99.9%) were obtained from Alfa Aesar. L-ascorbic acid and H<sub>2</sub>PtCl<sub>6</sub> were obtained from Sigma Aldrich. Indium tin oxide (ITO) coated glass slides (surface resistance 70–100 Ω sq<sup>-1</sup>, 25 mm × 25 mm) and glassy carbon plates (100 mm × 100 mm × 1 mm) were purchased from Sigma Aldrich and Alfa Aesar, respectively. Ethylene glycol was purchased from Fisher Scientific. The ITO-coated glass was cut into 6 mm × 6 mm pieces and the glassy carbon plates were cut into sizes of 50 mm × 10 mm, 50 mm × 2 mm, and 10 mm × 10 mm. Prior to use, the substrates were cleaned in acetone, ethanol, pure water and dried in N<sub>2</sub> gas. Bulk platinum wires used in the counter electrode were purchased from Alfa Aesar (0.5 mm diameter, annealed, 99.95% and 0.025 mm diameter, 99.95%). De-ionized water was used in all processing.

### 2.2. Ascorbic acid reduction process

A similar synthesis procedure as reported by Chang et al. was used in the present work [17]. All substrates were cleaned using the procedure described earlier. Pt nanoclusters were deposited using aqueous solutions of K<sub>2</sub>PtCl<sub>4</sub> of various concentrations. Also, the time of deposition was varied over a wide range. The concentrations of K<sub>2</sub>PtCl<sub>4</sub> in the solutions used were 10 mM, 15 mM, 20 mM, 40 mM, 60 mM, 80 mM, and 500 mM. The deposition process was conducted for 1 min, 5 min, 15 min, 30 min, 60 min, 90 min, and 120 min. While many conditions were used for synthesis, mainly to identify optimum conditions, most of the experiments were conducted only on a few selected samples. The procedure used for the synthesis was as follows: First 1 ml of the solution of the desired concentration of K<sub>2</sub>PtCl<sub>4</sub> was added to 36 ml of de-ionized water. Then the cleaned substrate was submerged into the solution. Next 2.0 ml of 100 mM ascorbic acid was added to the solution containing the substrate and maintained in the solution for the various times mentioned above. All depositions were carried out at room temperature. The samples were removed and rinsed in pure water several times and dried in N<sub>2</sub> gas. Characterization by FEI-SEM (FEI NanoNova), TEM (Tecnai F20 TEM/STEM/AFM), and electrochemical measurements were conducted on some of the prepared samples.

### 2.3. Polyol process

A similar synthesis procedure as reported by Sun et al. was used [18]. All substrates were cleaned using the procedure described earlier. A solution was prepared by dissolving 33 mg of H<sub>2</sub>PtCl<sub>6</sub> in 4 ml of ethylene glycol ( $\sim 20$  mM) while stirring for 5 min. The substrates were placed on a hotplate at 180 °C. Once the substrates reached 180 °C, the ethylene glycol solution was added drop-wise to the substrate until covered and was maintained for 5 min. After 5 min, a platinum nanocluster film had formed and all other products had evaporated. The samples were cooled to room temperature, rinsed with water, and dried in N<sub>2</sub> gas. Characterization by FEI-SEM (FEI NanoNova), TEM (Tecnai F20 TEM/STEM/AFM), and electrochemical measurements were conducted on some of the prepared samples.

### 2.4. Electrochemical measurements

A schematic of the cell used for electrochemical measurements is shown in Fig. 2. A 0.1 M PtCl<sub>4</sub> in DMSO electrolyte solution was used in all experiments. The working electrode was the deposited nanoclustered platinum on a substrate (glassy carbon or ITO-coated

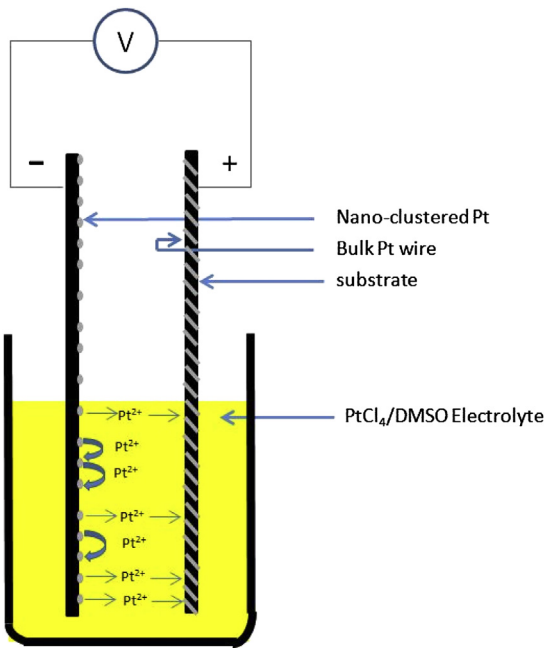


**Fig. 2.** A schematic of the experimental setup used with nanoclustered platinum as the working electrode, and bulk platinum wire as the counter electrode. The electrolyte was 0.1 M  $\text{PtCl}_4$  in DMSO.

glass) and the counter electrode was bulk platinum wire wrapped around either a glassy carbon or ITO substrate (to match the working electrode substrate). The spacing between the electrodes was either 1 mm or 6 mm. In this manuscript only the results on nanoclusters made by the polyol process are reported, since removing them from the substrates after electrochemical tests for subsequent TEM studies could be readily accomplished unlike nanoclusters made by the ascorbic acid method. Also, electrochemical testing was primarily done only with glassy carbon as the substrate, the results of which are reported here. Similar results are expected with ITO as the substrates since the main function of the substrate is to facilitate electron transport. Thus, the only requirements for the substrate are that it exhibits sufficient electronic conductivity (comparable to or preferably higher than the ionic conductivity of the electrolyte) and it remains inert in the liquid medium. Platinum wires of diameter 0.5 mm and 0.025 mm were used for 6 mm and 1 mm electrode spacing, respectively. The electrode assembly was partially dipped into the electrolyte solution, and connected to a Keithley 6514 high input impedance electrometer to measure the voltage between the electrodes. Data were collected using Labview software. Most of the measurements were conducted for 24 h, with some as long as 5 days and some as short as 2 h. In some cases, the electrolyte was stirred at 100 RPM using a small magnetic stirrer. After the measurements, the samples were rinsed and dried. The platinum nanoclusters were then either imaged directly using SEM, or scraped off onto a grid for TEM imaging.

### 3. Results and discussion

#### 3.1. Electron microscopy and particle size distributions

**Fig. 3** shows TEM images of platinum nanoclusters deposited directly onto TEM grids (Ted Pella, ultra-thin carbon on holey support) via ascorbic acid reduction of 60 mM  $\text{K}_2\text{PtCl}_4$  for 30 min. **Fig. 3(a)** shows a single nanocluster of approximately 100 nm in

diameter. The typical nanocluster size ranged between 50 nm and several hundred nm. **Fig. 3(b)** shows a higher magnification image of the nanocluster. As seen in the micrographs, the nanoclusters are comprised of very small nanoparticles. It was observed that the nanocluster size was a function of the  $\text{K}_2\text{PtCl}_4$  concentration and the deposition time. However, the size of the individual, smaller nanosize platinum particles within the nanoclusters was found to be independent of the concentration of  $\text{K}_2\text{PtCl}_4$  and the time of deposition. It was also observed that the nanoparticles within the nanoclusters were essentially of uniform size (narrow size distribution).

**Fig. 4** shows SEM images of platinum nanoclusters deposited on glassy carbon using the polyol process described earlier. **Fig. 4(a)** shows a low magnification image of the general morphology of the particles. As seen in the micrograph, the individual nanoclusters appear to be of a uniform size. **Fig. 4(b)** is a higher magnification image which shows a chain (necklace)-like structure formed of the nanoclusters. **Fig. 5(a)** and (b) are TEM images of the same sample. The TEM images show that the nanoclusters seen in **Fig. 4** are in fact composed of many smaller nearly spherical nanoparticles of approximately 5 nm in diameter. The lattice image along the periphery of the particles shows that these individual, smaller nanoparticles are single crystalline and are randomly oriented with respect to each other. That is, the inter-particle interfaces are high angle grain boundaries. The interior of the nanoclusters cannot be properly imaged due to the large thickness in the interior, away from the edges of the image. The morphology is interesting in that particles of ~5 nm diameter aggregate to form nanoclusters of ~50–300 nm in diameter, which then aggregate into a large network of chains several microns across. It seems that the platinum particles formed in the polyol process cease to grow individually past around 5 nm, but then favor clustering.

**Fig. 6** shows TEM images and particle size distribution histograms for the platinum nanoclusters deposited using the polyol process, in the as-deposited stage as well as after various electrochemical tests. Only the sizes of the nanoparticles on the surface of the nanoclusters could be measured as the interior regions could not be imaged due to the large thickness in the center. Fortunately, only the nanoparticles on the surface are subject to electrochemical growth and of interest in this study. However, this limited the number of particles to no more than about 250 that could be realistically measured.

**Fig. 6(A)** shows a TEM image of the platinum nanoparticles in the as-deposited state and the corresponding particle size distribution histogram. The corresponding average particle size (diameter) is 4.8 nm with a rather narrow size distribution (standard deviation of 0.6 nm). **Fig. 6(B)** shows a TEM image of the nanocluster tested for 24 h vs. a bulk platinum wire (0.5 mm diameter) in 0.1 M  $\text{PtCl}_4$ /DMSO electrolyte solution and the corresponding particle size distribution histogram. The average particle size is measured to be 5.17 nm with a standard deviation of 1 nm, indicating a modest increase in size and a slight broadening of the distribution. This suggests that some growth of the particles residing on the surface of the nanoclusters occurred which involved the dissolution of smaller particles and deposition on larger particles. **Fig. 6(C)** shows a TEM image and the corresponding particle size distribution histogram of a sample after an electrochemical test for 24 h in which the electrolyte solution was stirred at 100 RPM using a magnetic stirrer. The objective was to minimize the boundary layer and increase the kinetics of mass transport, which should lead to an increase in the kinetics of growth. In this case also very little growth was observed, with an average size (diameter) of 5 nm and a standard deviation of 0.75 nm, indicating a slight broadening of the distribution. These two experiments showed that very little growth occurred in 24 h, with or without stirring the

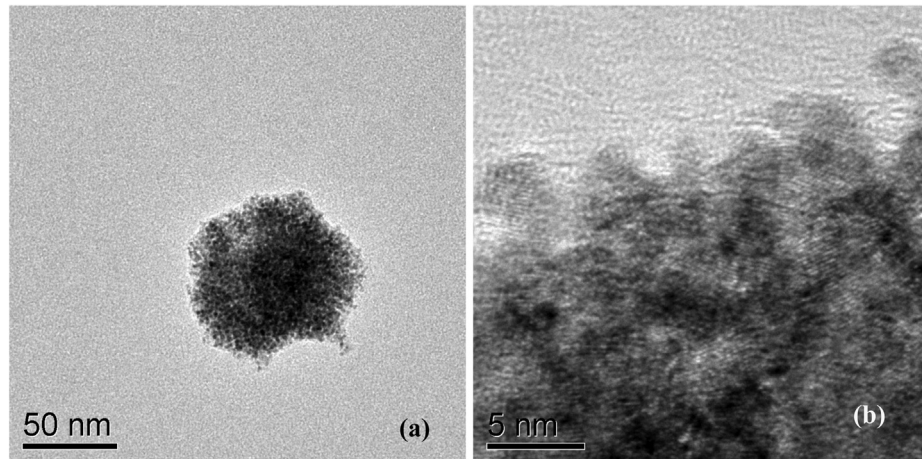


**Fig. 3.** TEM images of platinum nanoclusters deposited directly onto a TEM grid. Ascorbic acid reduction of 60 mM K<sub>2</sub>PtCl<sub>6</sub>, 30-min deposition time.

electrolyte. Fig. 6(D) shows a TEM image and the corresponding particle size distribution of a sample that had been tested in the same setup under static conditions (no stirring) for 5 days. In this case, some growth was observed, with the average particle size of 6.7 nm and the corresponding standard deviation of 1.65 nm, indicating broadening of the distribution.

Only the nanoparticles on the surface of the clusters are expected to undergo growth. This is because the nanoparticles on the surface are in contact with the electrolyte. Thus transport of Pt can occur as a coupled transport of Pt ions through the liquid, in which the diffusion coefficient is on the order of  $10^{-6}$  cm<sup>2</sup> s<sup>-1</sup>, and of electrons through the particles (through the nanocluster). The nanoparticles in the interior are not in contact with the electrolyte. Thus, transport among the nanoparticles in the interior can only occur by solid state diffusion, which is orders of magnitude sluggish at room temperature [15]. Investigation of the growth of surface nanoparticles in the nanoclusters thus also highlights the importance of this mechanism of catalyst degradation in PEM fuel cells in which the nanoparticles are in contact with liquid water. Fig. 7(a) and (b) shows schematics of the initial cluster, the cluster after some growth and the role of coupled transport in particle growth.

The increase in the average particle size in Fig. 6 represents a 40% increase compared to the as-deposited platinum. In some previous work using similar testing methods but using commercial

platinum catalysts (E-TEK) supported on high surface area carbon, significant growth was observed under similar conditions [19]. In the case of standard, carbon-supported platinum catalysts, 90% increase in particle size occurred in 24 h and over 300% increase occurred after 5 days, with the average particle size growing from the initial ~2.1 nm to ~8.5 nm [19]. By contrast, in the present work, the particle size grew from the initial 4.8 nm to only 6.7 nm under similar conditions. The difference is even more striking when considering the differences in the inter-particle distances in the two studies. In the present work, the inter-particle distance was small as the particles involved in growth were in direct contact. By contrast, in studies on Pt catalysts supported on carbon, the vast majority of the particles were not in contact with each other. That is, in that study the inter-particle distance was larger than in the present work [19]. Since the driving force for growth is inversely proportional to the distance of separation, it is expected that the effect of particle size distribution would be even greater if the inter-particle distance had been the same in the two studies. The preceding statement assumes that a quasi-steady state was not established during the course of the experiments insofar as the kinetics of growth is concerned. If a quasi-steady state is established, such as that assumed in the Lifschitz–Slyozov–Wagner (LSW) model, then the inter-particle spacing does not directly enter the equations of transport. More about this will be discussed later.

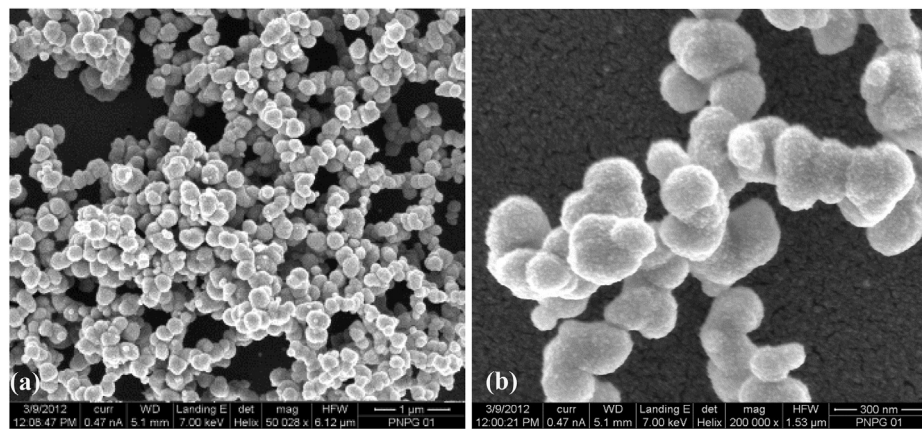


**Fig. 4.** SEM images of Pt deposited on glassy carbon by the polyol process using 20 mM H<sub>2</sub>PtCl<sub>6</sub> solution at 180 °C. Each of the clusters (~200 nm) has a noticeable roughness to the surface, which are actually agglomerates of ~5 nm Pt particles.

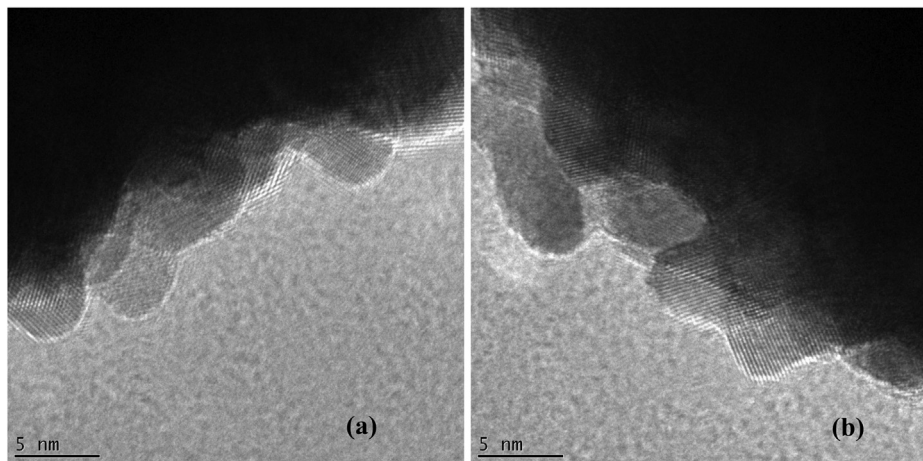


**Fig. 5.** TEM images of polyol-processed platinum nanoclusters deposited on glassy carbon and scraped off onto a TEM grid for imaging. Lattice images of the nanoparticles on the surface of the cluster are seen in the micrographs.

All histograms in Fig. 6 could be adequately fitted using normal distribution. In the LSW model which describes quasi-steady state Ostwald ripening, the distribution is LSW-type, which is different from the normal distribution. In quasi-steady state agglomeration, the expected distribution is lognormal. The observation in the present

work that the particle size distribution is neither LSW-type nor lognormal but can be described by normal distribution implies that quasi-steady state was probably never achieved. This also means that likely transport occurs between adjacent particles and that distance of separation between the adjacent particles may be important.

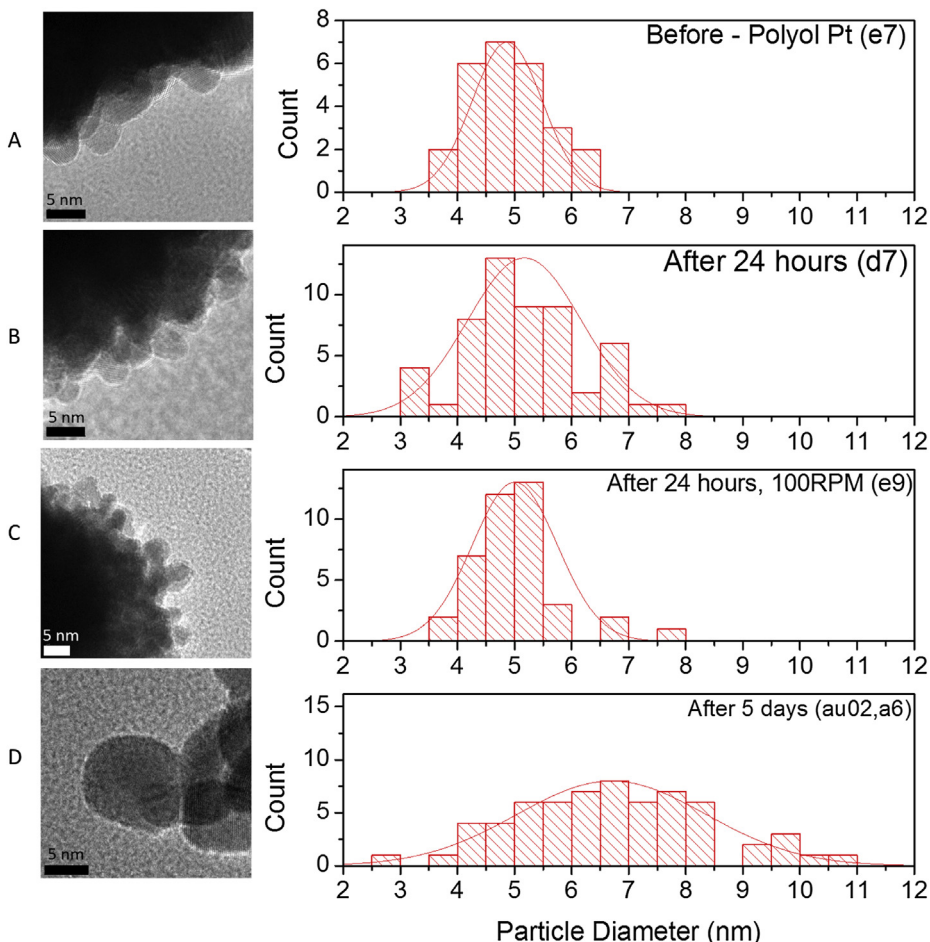


**Fig. 6.** TEM images and size distributions: (A) as-deposited platinum nanoclusters by the polyol process. Samples (B), (C), and (D) are also polyol deposited platinum nanoclusters and were tested in the electrochemical cell with 0.1 M  $\text{PtCl}_4/\text{DMSO}$  electrolyte vs. Pt wire (0.5 mm diameter) at 6 mm spacing. (B) was tested for 24 h without stirring, (C) was tested for 24 h with stirring at 100 RPM, and (D) was tested for 5 days without stirring.

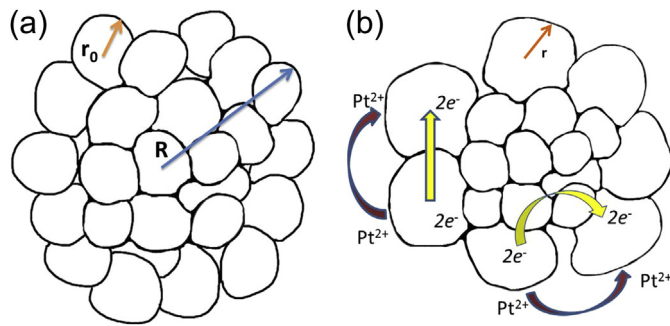


**Fig. 7.** (a) A schematic showing a cluster of nano-Pt particles.  $R$  is the cluster radius, and  $r_0$  is the initial radius of nanoparticles on the surface of the cluster. (b) A schematic showing the occurrence of growth of particles on the surface of the clusters by a coupled transport of  $\text{Pt}^{2+}$  through the liquid and  $2\text{e}^-$  through the cluster. The radius,  $r$ , of the nanoparticles on the surface increases with time.

### 3.2. Electrochemical measurements on polyol deposited Pt nanoclusters

Fig. 8 shows a voltage vs. time plot of an electrochemical cell in which both electrodes were identical; namely polyol deposited Pt nanoclusters on glassy carbon. Since both electrodes were identical, we expect the voltage between the two electrodes should be zero as identical processes occur at the two electrodes and are connected such that the effects of the processes at one electrode are cancelled out by the effects of processes occurring at the other electrode, insofar as measurements made in the external circuit are concerned. As seen in Fig. 8, after some initial transient, the voltage is indeed very close to zero. Small differences can occur due to small temperature changes/differences at the two electrodes and some convective effects. Initially, the measured voltage is positive. This may be due to the possibility that not both electrodes contacted the electrolyte at the same time during immersion. The electrode that was immersed first will develop positive or negative potential depending upon whether Pt ion transfer occurs from the electrolyte to the nano-electrode (deposition) or from the electrode into the electrolyte (dissolution). In the present work, the electrolyte was

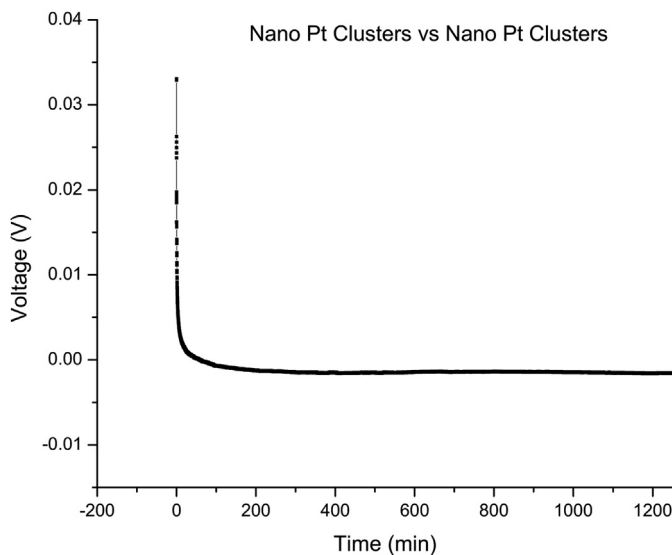


**Fig. 8.** A voltage vs. time plot for the electrochemical cell with both electrodes being polyol deposited Pt nanoclusters. The electrolyte solution was 0.1 M  $\text{PtCl}_4$  in DMSO. After the initial transient (due to small differences in the cell equilibration) the voltage stabilizes and is nearly zero.

$\text{PtCl}_4$  dissolved in DMSO. Prior work, however, has shown that the process of deposition or dissolution at a Pt electrode involves  $\text{Pt}^{2+}$  ions and not  $\text{Pt}^{4+}$  ions [20]. It was observed that even if the salt used is  $\text{PtCl}_4$ , the dominant electrode reactions involve  $\text{Pt}^{2+}$  ions as follows:  $\text{Pt} \rightarrow \text{Pt}^{2+} + 2\text{e}'$  (oxidation; anodic), and  $\text{Pt}^{2+} + 2\text{e}' \rightarrow \text{Pt}$  (reduction; cathodic) [20]. This is because when Pt is in contact with  $\text{PtCl}_4$ , the reaction  $\text{PtCl}_4 + \text{Pt} \rightarrow 2\text{PtCl}_2$  is expected to occur until equilibrium is established (at least locally). Since the solubility of  $\text{PtCl}_2$  is very small, this equilibrium is expected to be established with a relatively small concentration of  $\text{Pt}^{2+}$  ions. Transport thus occurs of  $\text{Pt}^{2+}$  from one electrode to the other electrode, even though the concentration of  $\text{Pt}^{4+}$  is much higher than that of  $\text{Pt}^{2+}$  [20]. It is also known that  $\text{PtCl}_4$  is more soluble than  $\text{PtCl}_2$  in both water and many polar liquids (e.g. DMSO). Thus, despite the predominant cationic species being  $\text{Pt}^{4+}$  in the electrolyte, electrode reactions involve  $\text{Pt}^{2+}$  [20]. For this reason, in the rest of the manuscript, it is assumed that all reactions involve  $\text{Pt}^{2+}$  ions.

Figs. 9 and 10 show voltage vs. time plots for the aforementioned electrode assemblies (polyol deposited Pt nanoclusters vs. bulk Pt wire, 0.1 M  $\text{PtCl}_4$ /DMSO, 6 mm spacing). Note that in these experiments, the processes occurring at the two electrodes in general are different which should lead to a measured nonzero voltage difference between the two electrodes. All three samples were deposited on glassy carbon substrates (50 mm × 2 mm × 1 mm). Fig. 9 shows voltage vs. time plots for two experiments, one tested for 24 h in a static electrolyte, and the other tested for 24 h with the electrolyte stirred at 100 RPM. Fig. 10 shows a voltage vs. time plot for the test conducted in a static electrolyte for 5 days. In both sets of experiments, the initial voltage was negative (with the positive of the electrometer connected to the bulk Pt electrode), which sharply increased and became positive. This may be characterized as a two-stage behavior. In an earlier study on commercial Pt catalyst supported on carbon, a three-stage behavior was observed [19]. We will first describe the three-stage behavior before discussing the present data.

The time dependence of the voltage in electrochemical studies conducted on commercial E-TEK Pt catalysts supported on carbon, especially in dilute solutions, can be described by *three consecutive/*

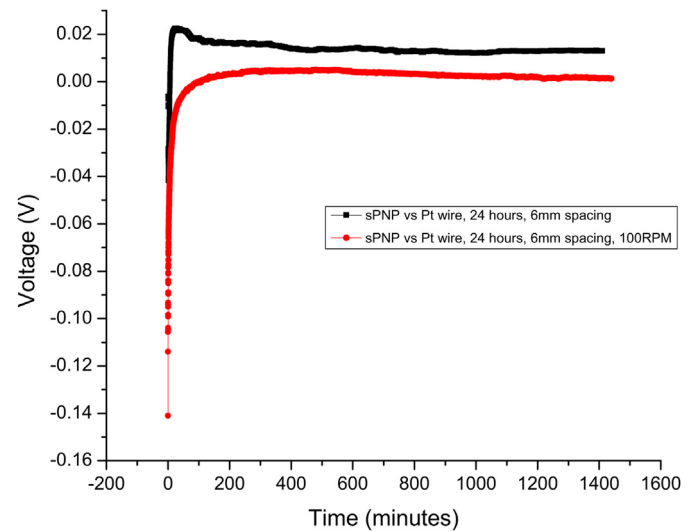


**Fig. 9.** Voltage vs. time plots for the electrode assemblies in 0.1 M  $\text{PtCl}_4$  + DMSO electrolyte solution. The positive of the electrometer was connected to the bulk Pt electrode. Thus, after the initial transients, the bulk Pt electrode is positive. The upper curve is for the sample of polyol deposited platinum nanoclusters tested over 24 h, and the lower curve is of the sample tested with the same setup but with the electrolyte stirred at 100 RPM. The positive of the electrometer was connected to the bulk Pt electrode. Thus, after the initial transients, the bulk Pt electrode is positive.

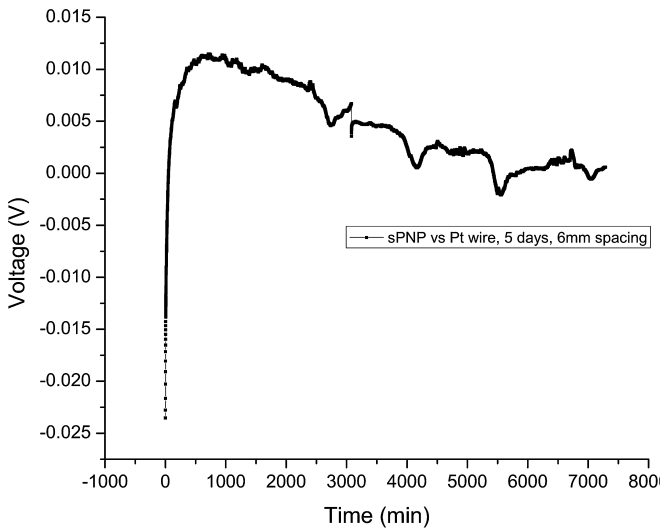


**Fig. 10.** A voltage vs. time plot for the electrode assembly in 0.1 M  $\text{PtCl}_4$  + DMSO electrolyte solution. The sample was polyol deposited platinum nanoclusters tested for 5 days. The positive of the electrometer was connected to the bulk Pt electrode. Thus, after the initial transients, the bulk Pt electrode is positive.

**concurrent stages** [19]. As soon as the electrodes are immersed in the electrolyte, in the first stage, we expect slight dissolution/precipitation will occur at the nano-Pt electrode/bulk Pt electrode. Note that the chemical potential of  $\text{Pt}^{2+}$  in the nanoparticles is higher than in the bulk Pt due to the surface energy effect (Gibbs–Thompson equation). Thus, as soon as the two electrodes are dipped in the electrolyte solution, one of the following three processes is expected to occur: (a) Dissolution of  $\text{Pt}^{2+}$  at both electrodes, with faster/greater dissolution at the nano-Pt electrode, wherein the  $\mu_{\text{Pt}^{2+}}^{\text{nano}} > \mu_{\text{Pt}^{2+}}^{\text{bulk}} > \mu_{\text{Pt}^{2+}}^{\text{electrolyte}}$ . This is expected in dilute solutions. This should make the nano-Pt electrode negative with respect to the bulk Pt electrode. (b) Deposition of  $\text{Pt}^{2+}$  from the electrolyte on both electrodes, with faster/greater deposition occurring on the bulk Pt, wherein  $\mu_{\text{Pt}^{2+}}^{\text{electrolyte}} > \mu_{\text{Pt}^{2+}}^{\text{nano}} > \mu_{\text{Pt}^{2+}}^{\text{bulk}}$ . This is expected in concentrated (super-saturated solutions). This too should make the nano-Pt electrode negative with respect to the bulk Pt electrode. (c) Dissolution of  $\text{Pt}^{2+}$  at the nano-Pt electrode and deposition of  $\text{Pt}^{2+}$  at the bulk Pt electrode, wherein  $\mu_{\text{Pt}^{2+}}^{\text{nano}} > \mu_{\text{Pt}^{2+}}^{\text{electrolyte}} > \mu_{\text{Pt}^{2+}}^{\text{bulk}}$ . This is expected in electrolyte solutions of intermediate concentrations. This should also make the nano-Pt electrode negative with respect to the bulk Pt electrode. Thus, as soon as the two electrodes are dipped into the electrolyte, we expect the nano-Pt electrode to become negative with respect to the bulk Pt electrode (assuming they are dipped into the electrolyte simultaneously). The kinetics of this step is expected to be very fast as no long range diffusion is expected. This would establish a slight gradient in  $\text{Pt}^{2+}$  concentration in the electrolyte between the two electrodes. Concurrently, the concentration gradient will tend to dissipate. During this stage the potential of the bulk Pt electrode will be positive with respect to the nano-electrode, and the potential will decrease with time. The higher the Pt salt concentration, the faster will be the kinetics of this stage. It was in fact noted that this stage could be observed for several seconds/minutes in dilute concentrations (0.01 M and 0.001 M) but could not be observed in electrolytes with higher concentrations (0.1 M) [19]. As seen in Figs. 9 and 10 in the present work also, this stage is not observed as the electrolyte concentration was rather high (0.1 M).

In each test (Figs. 9 and 10) there was a sharp increase in voltage from the initial voltage just after the two electrodes were dipped in

the electrolyte. This is the *second concurrent/consecutive stage*. The sharp change in voltage is indicative of a second transient stage in which  $\text{Pt}^{2+}$  ions transport from the platinum nanoclusters (nano-Pt electrode) to the bulk Pt wire due to the differences in the chemical potentials of Pt (and Pt ions) at the two electrodes. For  $\text{Pt}^{2+}$  the reaction at the nano-Pt electrode is  $\text{Pt} \rightarrow \text{Pt}^{2+} + 2e'$  (oxidation; anodic). The  $\text{Pt}^{2+}$  ions transport through the electrolyte to the bulk Pt wire (counter electrode), and the  $2e'$  transport through the external circuit. The transport of  $\text{Pt}^{2+}$  is expected to occur by diffusion as well as by natural convection. At the bulk Pt electrode the reaction is  $\text{Pt}^{2+} + 2e' \rightarrow \text{Pt}$  (reduction; cathodic). Since the measurements were made using a high impedance meter, negligible transport of electrons occurs, leading to the development of a (relative) positive potential on the bulk electrode, consistent with a sharp increase in voltage. Once the electrochemical potential of platinum ions, given by  $\tilde{\mu}_{\text{Pt}^{2+}} = \mu_{\text{Pt}^{2+}} + 2F\Phi$ , where  $\Phi$  is the electrostatic potential, is equilibrated in the two electrodes, a quasi-equilibrium is established. This is given by

$$\tilde{\mu}_{\text{Pt}^{2+}}^{\text{nano}} = \mu_{\text{Pt}^{2+}}^{\text{nano}} + 2F\Phi^{\text{nano}} = \tilde{\mu}_{\text{Pt}^{2+}}^{\text{bulk}} = \mu_{\text{Pt}^{2+}}^{\text{bulk}} + 2F\Phi^{\text{bulk}} \quad (1)$$

The measured voltage between the two electrodes, once a quasi-equilibrium has been reached, is thus given by

$$\begin{aligned} \Phi^{\text{bulk}} - \Phi^{\text{nano}} &= \frac{(\mu_{\text{Pt}^{2+}}^{\text{nano}} - \mu_{\text{Pt}^{2+}}^{\text{bulk}})}{2F} = \frac{(\mu_{\text{Pt}}^{\text{nano}} - \mu_{\text{Pt}}^{\text{bulk}})}{2F} \\ &= \frac{(\mu_{\text{Pt}}^{\text{nano}} - \mu_{\text{Pt}}^0)}{2F} \end{aligned} \quad (2)$$

Since the Fermi levels in both nano-Pt and bulk Pt are identical,  $(\mu_{\text{Pt}^{2+}}^{\text{nano}} - \mu_{\text{Pt}^{2+}}^{\text{bulk}})$  can be replaced by  $(\mu_{\text{Pt}}^{\text{nano}} - \mu_{\text{Pt}}^{\text{bulk}})$ . Additionally, as the bulk Pt was pure Pt,  $\mu_{\text{Pt}}^{\text{bulk}}$  is replaced by  $\mu_{\text{Pt}}^0$ , which is the standard state chemical potential of Pt.

The *third concurrent/consecutive stage* in the process is the occurrence of particle growth (Ostwald ripening/agglomeration sintering) in the nanoclustered platinum electrode, leading to a gradual decrease in voltage as seen in both Figs. 9 and 10. These three stages are depicted schematically in Fig. 11, along with their respective schematic voltage versus time trends. During the third stage, the electrochemical potentials of  $\text{Pt}^{2+}$  are essentially identical in the two electrodes, as given by Eq. (1). The difference in the measured voltage between the two electrodes thus gives a measure of the difference in the chemical potentials of Pt in the two electrodes (Eq. (2)). In all three stages, the bulk electrode is expected to be positive and the nano-electrode is expected to be negative, assuming the absence of any other effects such as slightly different temperatures at the two electrodes and/or the possible effects of differences in stresses. The measured voltage difference thus in principle can be related to the particle size in the n-Pt electrode.

The above discussion is based on the premise that both electrodes are immersed in the liquid electrolyte exactly at the same time and the liquid contacts Pt in both electrodes exactly at the same time. Under such conditions, the Pt bulk electrode should always be positive (as schematically shown in Fig. 11) and the n-Pt electrode should always be negative. However, we note that in both Figs. 9 and 10, the initial voltage was negative (with the positive of the meter connected to the bulk Pt electrode) which rapidly increased and became positive. A negative voltage is expected if the two electrodes do not contact the liquid electrolyte exactly at the same time. For example, if the bulk Pt electrode contacts the liquid before the nano-electrode (that is n-Pt from the nano-electrode) does (it is assumed that glassy carbon from the nano-electrode contacts the electrolyte before n-Pt does), flux of  $\text{Pt}^{2+}$  is expected from the bulk Pt electrode to the glassy carbon portion of the nano-electrode that has contacted the electrolyte. In such a case the

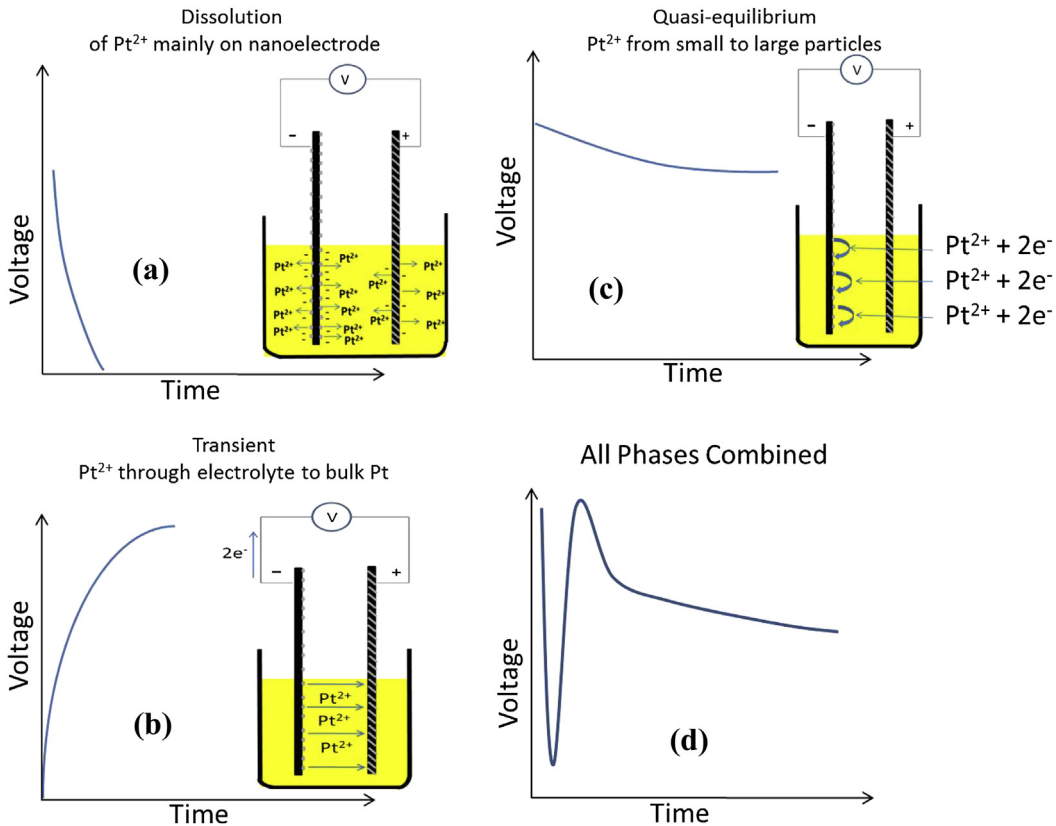


**Fig. 11.** Schematics showing the three stages observed when a nano-Pt electrode and a bulk Pt electrode are immersed in a Pt-salt electrolyte solution. (a) Rates of transfer of Pt<sup>2+</sup> to/from the electrodes from/to the electrolyte solution are different due to vastly different specific surface areas. These differences lead to a potential difference between the two electrodes. (b) In the second stage, Pt<sup>2+</sup> ions transport from the nano-Pt electrode to the bulk Pt electrode due to the higher chemical potential of Pt in the nano-Pt electrode compared to that in the bulk Pt electrode. This leads to an increase in the potential difference between the two electrodes. (c) A quasi-equilibrium state is achieved when the electrochemical potential of Pt<sup>2+</sup> is about the same in the nano-Pt and bulk Pt electrodes, which represents the third stage. In this stage, Ostwald ripening continues in the nano-Pt electrode. This is reflected as a gradual decrease in the voltage. (d) The schematic shows the overall expected time dependence of the observed voltage.

nano-electrode will initially become positive with respect to the bulk Pt electrode. The initially observed negative voltage in both Figs. 9 and 10 is thus attributed to this effect. In order to verify this hypothesis, the following experiment was conducted.

Pt wires were wrapped around two graphite rods. On one rod, the Pt wire was wrapped over the entire length. On the other rod, approximately 7 mm portion at one end (the end that would be immersed in the electrolyte) was left bare and Pt wire was wrapped on the rest of the length of the rod. The two rods were attached to a plastic holder. Then, with an electrometer connected to the rods, the rods (electrodes) were immersed in a 0.1 M PtCl<sub>4</sub> + DMSO electrolyte solution. In one experiment, the positive of the electrometer was connected to the electrode with the shorter Pt wire. As soon as the electrodes were immersed (Fig. 12) such that Pt from one electrode contacted the electrolyte but only the graphite from other electrode contacted the electrolyte, the measured potential was positive (initially about 4 mV) which sharply decreased (actually became slightly negative) and then approached zero voltage as eventually Pt from both electrode contacted the electrolyte (in about 10 s). The rationale is that as soon as the rods are dipped in the electrolyte, greater transfer of Pt<sup>2+</sup> will occur from the solution to the bare graphite electrode than can occur at the bulk Pt electrode due to differences in the Pt chemical potentials. Once both electrodes immersed such that both Pt wires contacted the electrolyte, both electrodes can be treated as being identical, and we expect the voltage between the two to be zero once equilibration has been achieved. The upper voltage vs. time trace in Fig. 12 shows the corresponding data. Note that after about 20 min,

the potential difference between the two electrodes is nearly zero as expected.

In the second experiment, the negative of the electrometer was connected to the electrode with the shorter Pt wire. In this case also as soon as the rods contact the electrolyte, greater transfer of Pt<sup>2+</sup> will occur from the solution to the bare graphite electrode due to differences in Pt chemical potentials. In this case also, the two rods were immersed (in about 10 s) such that eventually both Pt wires contacted the electrolyte solution, making both electrodes identical. As the polarities of the electrometer were reversed, the initial voltage was negative (~−10 mV) which sharply increases and eventually approaches zero (lower trace in Fig. 12). This experiment showed that in fact the sign of the observed initial voltage depends on which electrode contacts the liquid first (it is understood naturally that for the measurement of some voltage electrical contact of both rods with the electrolyte must occur). Based on this experiment, it is deduced that in both Figs. 9 and 10, the bulk Pt electrode must have contacted the liquid first. The initial rapid transients thus depend upon other factors, such as which electrode contacts the electrolyte first.

Fig. 9 shows that the potential rises sharply to a peak followed by a gradual decrease in a static electrolyte solution. When the solution is stirred, the potential rise is just as rapid. However, the voltage does not exhibit a sharp peak. This difference is attributed to the differences in mass transfer effects. In both cases, after the peak, the potential slowly decreases. The slow decrease is consistent with negligible increase in particle size as seen in Fig. 6(B) and (C). For the test conducted in a static electrolyte for 5 days, the shape of the

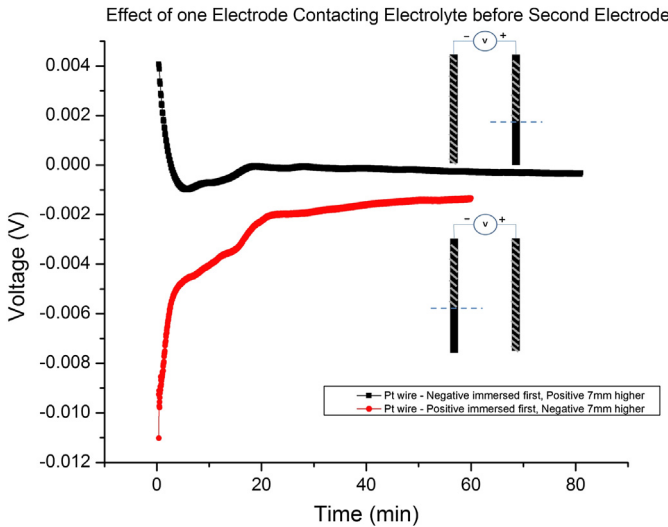


**Fig. 12.** Measurement of potential difference between two Pt bulk electrodes (Pt wire wrapped around graphite rods substrates) when immersed in  $\text{PtCl}_4 + \text{DMSO}$  electrolyte. On one electrode the Pt wire was wrapped all the way up to the bottom end. On the other, the Pt wire was wrapped up to about 7 mm from the bottom. Thus, as the two electrodes were inserted into the electrolyte solution, not both Pt wires contacted the electrolyte solution at the same time. The upper trace corresponds to the positive terminal of the meter connected to the electrode with shorter Pt wire. The lower trace corresponds to the positive terminal of the meter connected to the electrode with the longer Pt wire. Note the differences in the polarities of the voltage measured in the initial stages. After a long period of time, the measured voltage approaches zero as both electrodes are identical.

voltage vs. time plot is similar. However, the potential drop over the duration is larger than in Fig. 9, consistent with the greater growth observed in 5 days as compared to that in one day. Even so, as stated earlier, the growth is much slower than in commercial Pt supported on carbon, and consistent with a modest decrease in voltage observed in Fig. 10 even after 5 days compared to that observed when conventional commercial catalyst is used [19].

### 3.3. Effect of particle size distribution on the kinetics of growth

The observation that the kinetics of growth in the nanoclustered platinum is much slower than in n-Pt supported on carbon may in part be explained on the basis of the effect of particle radius on the chemical potential and the role of the initial size distribution on growth kinetics. The chemical potential of platinum in a single crystal isolated particle of radius  $r$  is given by [16]

$$\mu_{\text{Pt}}(r) = \mu_{\text{Pt}}^0 + \frac{2\gamma_{\text{sl}}}{r} V_M \quad (3)$$

where  $\mu_{\text{Pt}}^0$  is the chemical potential of pure, bulk Pt,  $\gamma_{\text{sl}}$  is the Pt–liquid solution surface energy,  $r$  is the particle radius, and  $V_M$  is the molar volume of platinum. Eq. (3) is for an isolated particle immersed in the liquid. In the present case, the particles are clusters of nanosize Pt particles. The boundaries between the adjacent particles are incoherent boundaries. If the grain boundary energy for incoherent boundaries is given by  $\gamma_{\text{gb}}$ , the approximate average surface energy of the particles residing on the surface of the nanoclusters may be given by

$$\gamma \approx \frac{A_{\text{sl}}\gamma_{\text{sl}} + A_{\text{gb}}\gamma_{\text{gb}}}{A_{\text{sl}} + A_{\text{gb}}} \quad (4)$$

where  $A_{\text{sl}}$  and  $A_{\text{gb}}$  are respectively the solid–liquid and the grain–grain surface areas of the nanosize particles on the surface of the

nanoclusters. As the average radius of the (surface) particle increases, its chemical potential decreases. For two particles of differing radii, the driving force for the growth of the larger particle and the shrinkage of the smaller particle is proportional to the difference in their chemical potentials and inversely proportional to the distance of separation. This statement assumes that a quasi-steady state distribution, typically assumed in Ostwald ripening models such as Lifschitz–Slyozov–Wagner (LSW) (or agglomeration/sintering models), has not been achieved. In the present work, the observed distribution is neither LSW nor lognormal, which suggests that a quasi-steady state was probably never achieved. In the LSW model (or models describing quasi-steady state agglomeration/sintering), the inter-particle distance does not directly enter growth kinetics (which are effectively mean field models). The models assume a mean concentration of the diffusing species in the medium. Then, diffusion of species occurs from a particle to the medium (when the particle is smaller than that corresponding to the mean concentration) or from the medium to a particle (when the particle is larger than that corresponding to the mean concentration). If a quasi-steady state has not been established, however, one may consider transport occurring from a smaller particle to an adjacent larger particle. In such a case, inter-particle spacing may need to be explicitly included in the transport equations.

In the nanoclusters of platinum investigated in the present work, the kinetics of growth of one particle (and the associated shrinkage of the other) will primarily involve adjacent particles. If their radii can be given as  $r + \Delta r$  and  $r - \Delta r$ , the corresponding chemical potentials are given by

$$\mu_{\text{Pt}}(r \pm \Delta r) = \mu_{\text{Pt}}^0 + \frac{2\gamma}{(r \pm \Delta r)} V_M \quad (5)$$

The corresponding difference in the chemical potentials, which is the driving force for the growth of one and the shrinkage of the other, is given by

$$\Delta\mu_{\text{Pt}} = \frac{2\gamma}{r - \Delta r} V_M - \frac{2\gamma}{r + \Delta r} V_M = \frac{4\gamma\Delta r}{r^2 - (\Delta r)^2} V_M \quad (6)$$

As the  $\Delta r$  goes to zero, so does the chemical potential difference, eliminating the driving force for particle growth. Fig. 6(A) shows that the initial particle size distribution is relatively narrow, with a standard deviation of 0.6 nm (small  $\Delta r$ ). Even after 5 days in a static electrolyte, the size increased to 6.7 nm with a standard deviation of 1.65 nm. By contrast, in commercial n-Pt supported on carbon, the initial average particle size was 2.1 nm but with a standard deviation of 1.4 nm (relatively large  $\Delta r$ ) [19]. These nano-Pt particles under similar conditions grew to a size of 8.5 nm with a standard deviation of 7.9 nm [19].

The present results thus demonstrate the profound role of the initial size distribution on the kinetics of growth. Indeed, in the study by Popescu et al., it was observed that gold particles (size-selected atom clusters) of initially broader size distribution grew at a significantly greater rate than gold particles of nearly identical size [13]. In fact, Popescu et al. [13] observed that mono-dispersed Au atom clusters containing 4 atoms or 6 atoms grew at a slower rate than Au atom clusters of a wider distribution, containing between 10 and 20 atoms. That is, particles of initially larger average size actually grew at a faster rate because of the wider distribution, resulting in greater thermodynamic driving force than particles of a smaller size, but of a narrower distribution. These results demonstrate the profound role of the initial particle size distribution on the kinetics of growth.

In the work by Popescu et al. [13], the atom clusters were size selected with a definite number of atoms in the clusters. Also, the

clusters were well-dispersed and not in physical contact with each other. Thus, a crude estimate of the thermodynamic driving force can be obtained. Approximating each atom cluster as a sphere, the radius of a given cluster  $r_c$  is proportional to the cube root of the number of atoms,  $N_c$  in the atom cluster; that is  $r_c = aN_c^{1/3}$  where  $a$  is a geometric shape factor. For growth/shrinkage of two atom clusters with one cluster containing  $N_{c(1)}$  atoms and the other cluster containing  $N_{c(2)}$  number of atoms, the average cluster radius is  $\bar{r}_c = a(N_{c(1)} + N_{c(2)})^{1/3}$ , assuming the same shape factor regardless of the number of atoms in a cluster. Thus, the difference in chemical potentials of the two clusters is given by

$$\Delta\mu(r_1, r_2) = \Delta\mu(N_{c(1)}, N_{c(2)}) \\ = k \frac{\left(N_{c(1)}^{1/3} - N_{c(2)}^{1/3}\right)}{\left[\left(\frac{N_{c(1)} + N_{c(2)}}{2}\right)^{2/3} - \left(N_{c(1)}^{1/3} - N_{c(2)}^{1/3}\right)^2\right]} \quad (7)$$

where  $k = 4\gamma V_M/a$  is a constant. Substituting  $N_{c(1)} = 6$  and  $N_{c(2)} = 4$  gives  $\Delta\mu(6,4) = 0.08k$  and substituting  $N_{c(1)} = 20$  and  $N_{c(2)} = 10$  gives  $\Delta\mu(20,10) = 0.1017k$ . Indeed, the difference in the chemical potentials on an absolute basis between clusters containing between 10 and 20 atoms is larger than the difference in chemical potentials between clusters containing between 4 and 6 atoms. Thus, we expect the kinetics of coarsening of the clusters containing between 10 and 20 atoms to be faster than the kinetics of the clusters containing between 4 and 6 atoms, in accord with the observations of Popescu et al. [13]. Fig. 13(a) shows the calculated  $\Delta\mu(r_1, r_2)$  using Eq. (7). In Fig. 13(a) calculated  $\Delta\mu(N_{c(1)}, N_{c(2)})$  for three values of the total number of atoms in the two particles, namely  $N_c = (N_{c(1)} + N_{c(2)})$ , with  $N_c = 10, 20$ , and  $40$  are shown. Note that depending upon the total number of atoms in a cluster and the possible range, the  $\Delta\mu(N_{c(1)}, N_{c(2)})$  can vary over a wide range. For example, for  $N_c = 40$ , the  $\Delta\mu(N_{c(1)}, N_{c(2)})$  varies by over two orders of magnitude. Indeed, the role of the initial particle size distribution is expected to be profound. The observations of Popescu et al. on gold size-selected atom clusters [13], the present work on nanosize Pt particles of narrow size distributions, and the above calculations show that the narrower the particle size distribution, the slower should be the kinetics of coarsening.

In the work by Popescu et al. [13], gold particles were very small size-selected atom clusters containing up to about 20 atoms. In most PEM fuel cells, Pt catalyst particles are on the order of a few nm in size, containing hundreds to thousands of atoms. In order to assess the effect of particle size distribution on chemical potential difference (and thus on the kinetics of degradation), calculations were made on particles on the order of a few nm in size. Fig. 13(b) shows the calculated values of  $\Delta\mu(r_1, r_2)$  for two sets of particles. The curve in black corresponds to  $N_c = (N_{c(1)} + N_{c(2)}) = 642$ . If the two particles are of identical size, their diameters would be 2.1 nm (radii of 1.05 nm). The corresponding  $\Delta\mu(r_1, r_2)$  would be zero. The figure thus shows  $\Delta\mu(r_1, r_2)$  for the smallest difference in the number of atoms (size) selected here in which  $r_1 = 1.045$  nm and  $r_2 = 1.055$  nm. The corresponding normalized  $\Delta\mu(r_1, r_2)$  is  $\sim 1.3 \times 10^{-3}$ . If the particle radii had been  $r_1 = 0.425$  nm and  $r_2 = 1.31$  nm, the corresponding normalized  $\Delta\mu(r_1, r_2)$  would be  $\sim 0.4$ , which is more than two orders of magnitude larger, thus showing a profound effect of particle size distribution on the thermodynamic driving force for growth (degradation). The curve in red corresponds to  $N_c = (N_{c(1)} + N_{c(2)}) = 7664$  atoms. If the two particles are of identical size, their diameters would be 4.8 nm (radii of 2.4 nm). The figure only shows calculations for a range up to 2800 atoms (difference in the two particles), which corresponds to a maximum difference corresponding to  $r_1 = 2.1$  nm and

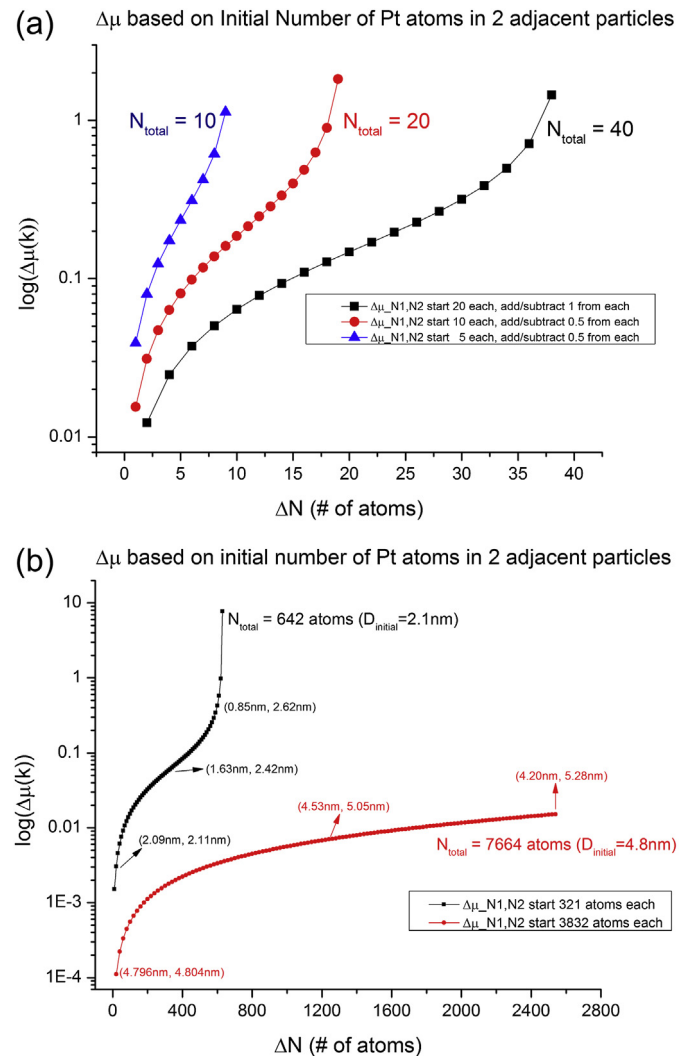


**Fig. 13.** (a) Plots of  $\Delta\mu(r_1, r_2)$  (on a logarithmic scale) vs.  $\Delta N$  for two particles with a fixed total number of atoms:  $N = 10, N = 20$  and  $N = 40$ . Note that the  $\Delta\mu(r_1, r_2)$  can vary by  $\sim 2$  orders of magnitude for the values of  $N$  selected here. (b) Plots of  $\Delta\mu(r_1, r_2)$  (on a logarithmic scale) vs.  $\Delta N$  for two particles with a fixed total number of atoms: (i) the curve in black corresponds to two Pt particles containing a total of 642 atoms. If the two particles were of identical size, their diameters would have been 2.1 nm (radii of 1.05 nm). (ii) The curve in red corresponds to two Pt particles containing a total of 7664 atoms. If the two particles were of identical size, their diameters would have been 4.8 nm (radii of 2.4 nm). Note that  $\Delta\mu(r_1, r_2)$  varies over three orders of magnitude for the ranges given. (For interpretation of the references to colour in this figure legend, the reader is referred to the web version of this article.)

$r_2 = 2.64$  nm. Over this range, that is from  $(r_1 = 2.398$  nm,  $r_2 = 2.402$  nm) to  $(r_1 = 2.1$  nm,  $r_2 = 2.64$  nm), the thermodynamic driving force for growth (degradation) varies by over two orders of magnitude. Indeed, the initial particle size difference is expected to have a very profound effect on the kinetics of catalyst degradation.

The nanoclusters of platinum examined in this study are not suitable as catalysts since a large amount of platinum, which is in the interior of these clusters, cannot participate in any catalytic or electro-catalytic reactions. Also, the kinetics of growth of surface particles in the clusters investigated here is expected to be somewhat slower than isolated particles since the grain boundary energy,  $\gamma_{gb}$  is expected to be lower than  $\gamma_{s-vapor}$ . However, depending on the type and the concentration of any adsorbed species from the liquid,  $\gamma_{sl}$  may be larger or smaller than  $\gamma_{gb}$ . In either case, the relevant particle size is the particle radius,  $r$ , and not the cluster radius,  $R$ . Fig. 7(a) shows the distinction between the two radii.

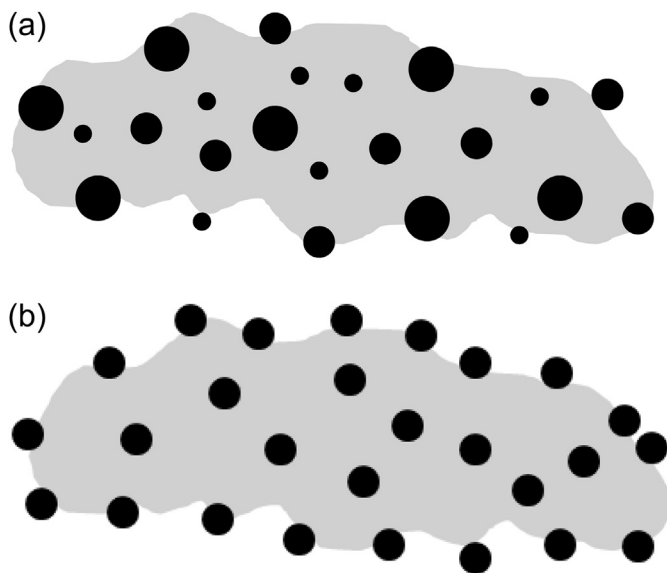


**Fig. 14.** (a) Typical, commercial Pt catalyst supported on carbon with a relatively wide size distribution. The greater the variation in the sizes of the particles (wider the size distribution), the faster is the kinetics of catalyst degradation. (b) Desired mono-dispersed Pt catalyst supported on carbon. Such catalyst particles should be highly resistant to degradation.

Despite these differences, the results of the present work show that the desired catalysts for applications such as PEMFC from the standpoint of durability should be mono-dispersed.

In the work by Popescu et al. [13], sub-nano to nanoclusters of Au deposited on carbon were aged at room temperature. Since no electrolyte solution was present in their work [13], growth of Au clusters likely occurred by surface diffusion of Au atoms along the surface of carbon [13]. Solid state diffusion of Au at room temperature is expected to be rather sluggish, consistent with their observations that growth continued to occur for nearly 3 years. In the present studies and in PEMFC, nanoparticles of Pt supported on carbon are immersed in a liquid medium and an ionomer, and growth occurs by a coupled transport of ions through liquid/ionomer and electrons through the supporting carbon. Since diffusion is fast in liquids, the kinetic factor that dictates growth kinetics of PEMFC electrodes is the Pt ion concentration. The thermodynamic factor that dictates growth kinetics is the difference in particle sizes. Thus, the present work suggests that efforts need to be devoted towards the synthesis of carbon-supported platinum (or platinum alloy catalysts) that are mono-dispersed, that is, with a very narrow size distribution. Fig. 14(a) shows a schematic of a typical, commercially available, Pt catalyst supported on carbon with a rather wide distribution. The greater the variation in particle size (wider the size distribution), the faster will be the kinetics of degradation. Fig. 14(b) shows a schematic of the desired mono-dispersed Pt catalyst supported on carbon. Such catalysts should be highly resistant to degradation by growth. Calculations presented in Fig. 13(b) provide an approximate yet a quantitative basis for the design of degradation-resistant catalysts for PEMFC.

#### 4. Conclusions

Nanoclustered platinum particles were synthesized using two processes; one involving the use of  $K_2PtCl_4$  and ascorbic acid, and the other involving  $H_2PtCl_4$  and polyol [17,18]. The nanoclusters were formed by direct deposition on glassy carbon and ITO-coated glass substrates. The resulting nanoclusters of Pt consisted of

nano-particles of 4–5 nm in diameter with a narrow particle size distribution. Electrochemical growth of the individual particles on the surface of the nanoclusters was investigated using an electrochemical cell. One electrode in the cell comprised of platinum wire wrapped on a substrate (glassy carbon or ITO) and the other electrode consisted of Pt nanoclusters deposited on a similar substrate. The electrode assembly was immersed in 0.1 M  $PtCl_4$  + DMSO electrolyte solution. The voltage between the two electrodes was measured as a function of time. After the initial transients (stages 1 and 2) the voltage between the two electrodes slowly decreased (stage 3). The difference in voltage between the two electrodes during stage three is related to the particle size of n-Pt particles in the nanoclusters of Pt in the nano-electrode. The third stage is characterized by the occurrence of particle growth (Ostwald ripening) on the nanoclustered Pt electrode. As the particle growth occurred, the chemical potential of Pt in the nanoclustered electrode decreased, which resulted in a decrease in the measured voltage. Samples were subsequently examined under a TEM to determine the size and the size distributions. It was observed that particle growth was less pronounced compared to commercial n-Pt supported on carbon tested under similar conditions [19].

The principal difference between the as-prepared nanoclusters of Pt in this study and the commercially available n-Pt supported on carbon is the difference in their size distributions. In commercial n-Pt catalysts, the initial size distribution is relatively broad. This leads to a greater difference in the chemical potentials between adjacent particles, thus leading to faster growth kinetics due to the larger driving force. By contrast, the initial size distribution of nanoparticles of Pt in the samples synthesized in the present work was relatively narrow, leading to a smaller difference in chemical potentials, and thus leading to slower growth kinetics. The present work suggests that if carbon-supported n-Pt catalysts can be prepared with very narrow particle size distributions, their stability in devices such as PEMFC may be substantially improved.

#### Acknowledgments

This work was supported in part by the National Science Foundation under Grant Number CBET-0931080 and in part by NSF-MRSEC Grant No. DMR 11-21252. The authors acknowledge the assistance of all members of our lab as well as those in the TEM lab at Brigham Young University.

#### References

- [1] M.S. Wilson, F.H. Garzon, K.E. Sickhaus, S. Gottesfeld, *J. Electrochem. Soc.* 140 (10) (1993) 2872–2877.
- [2] R. Ornelas, A. Stassi, E. Modica, A.S. Arico, V. Antonucci, *ECS Trans.* 3 (1) (2006) 633–641.
- [3] X. Wang, R. Kumar, D. Meyers, *J. Electrochem. Solid State Lett.* 9 (5) (2006) A225–227.
- [4] J. Xie, D.L. Wood III, K.L. More, P. Atanassov, R.L. Borup, *J. Electrochem. Soc.* 152 (5) (2005) A1011–A1020.
- [5] P.J. Ferreira, G.J. Lao, Y. Shao-Horn, D. Morgan, R. Makaria, S. Kocha, H.A. Gasteiger, *J. Electrochem. Soc.* 152 (11) (2005) A2256–A2271.
- [6] W. Bi, G.E. Gray, T.F. Fuller, *Electrochim. Solid-State Lett.* 10 (5) (2007) B101–B104.
- [7] K. Yasuda, A. Taniguchi, T. Akita, Z. Siroma, *Phys. Chem. Chem. Phys.* 8 (2006) 746.
- [8] A. Ohma, S. Suga, S. Yamamoto, K. Shinohara, *Proton Exchange Membrane Fuel Cells 6*, in: T. Fuller, et al. (Eds.), *ECS Trans.*, vol. 3(1), 2006, pp. 519–529.
- [9] H. Liu, J. Zhang, F.D. Coms, W. Gu, B. Litteer, H.A. Gasteiger, *Proton Exchange Membrane Fuel Cells 6*, in: T. Fuller, et al. (Eds.), *ECS Trans.*, vol. 3(1), 2006, pp. 493–505.
- [10] A. Lacontti, H. Liu, C. Mittelstaedt, R. McDonald, in: T. Jarvi, et al. (Eds.), *ECS Trans.*, vol. 1(8), 2005, pp. 199–219.
- [11] B. Merzougui, S. Swathirajan, *J. Electrochem. Soc.* 153 (12) (2006) A2220–A2226.
- [12] K.L. More, R. Borup, K.S. Reeves, *ECS Trans.* 3 (1) (2006) 717–733.
- [13] R. Popescu, R. Schneider, D. Gerthsen, A. Bottcher, D. Loffler, P. Weis, M.M. Kappes, *Surf. Sci.* 603 (2009) 3119–3125.

- [14] A.V. Virkar, Y. Zhou, *J. Electrochem. Soc.* 153 (6) (2007) B540–B547.
- [15] M.L. Marcos, J.G. Velasco, *Chem. Phys. Lett.* 282 (1998) 391–394.
- [16] O.W. Devereaux, *Topics in Metallurgical Thermodynamics*, A Wiley-Interscience Publication, New York, 1983.
- [17] G. Chang, M. Oyama, K. Hirao, *J. Phys. Chem. B* 110 (2006) 1860–1865.
- [18] K. Sun, B. Fan, J. Ouyang, *J. Phys. Chem. C* 114 (2010) 4237–4244.
- [19] P. Parthasarathy, A.V. Virkar, *J. Power Sources* 234 (2013) 82–90.
- [20] P. Parthasarathy, A.V. Virkar, *J. Power Sources* 196 (2011) 9204–9212.